

Health Issues Concerning Carbon-TiO₂ Nanomaterials Produced by Flame Synthesis

Gianluigi De Falco^a, Mario Commodo^b, Paola Pedata^c, Patrizia Minutolo^b, Andrea D'Anna^a

^aDipartimento di Ingegneria Chimica, dei Materiali e della Produzione Industriale, Università degli Studi di Napoli Federico II, P.le Tecchio 80, 80125, Napoli, Italy

^bIstituto di Ricerche sulla Combustione, CNR, P.le Tecchio 80, 80125, Napoli, Italy

^cDipartimento di Medicina Sperimentale – Sezione di Igiene, Medicina del Lavoro e Medicina Legale, Seconda Università di Napoli, Via L. De Crecchio 7, 80138 Napoli, Italy

gianluigi.defalco@unina.it

Titanium dioxide TiO₂ is one of the most important and most used materials in the modern era. Because of its properties it is suitable for a large number of applications in several different fields. In the bulk phase, it is primarily used as a white pigment. As nanomaterial, it is a component in dye-sensitized and organic solar cells as well as in food and personal care products. In the last years personal care applications are increasing; for example nano-powdered TiO₂ is extensively employed as physical filter in commercial sunscreens, since it is capable to adsorb and scatter both UVA and UVB radiations and to eliminate the natural opacity typical of microsized sunscreens. However, together with its physical and chemical properties, it is important to assess health implications that the use of TiO₂ powder in the nanometer scale might have in personal care applications. A possible way to reduce health implications, especially when related to the formation of free-radicals, is given by coating and doping of TiO₂ nanoparticles with organic and inorganic additives. Different efficiencies in preventing the release of free radicals can be achieved, depending on the nature of coating and doping. In this work, the formation of pure TiO₂ nanoparticles and carbon-titania nanocomposite by flame synthesis is presented. The procedure is based on the injection of Ti precursor solutions inside hydrocarbon flames with different equivalent ratios. This allows us to synthesize nano-sized particles (1-10 nm), with specific crystallinity phase and carbon content. Chemical and physical properties, composition and dimension of flame-synthesized nanoparticles are characterized by Raman spectroscopy, UV-visible light absorption and Atomic Force Microscopy. Analysis of Reactive Oxygen Species in human keratinocytes cellular lines is used to select the operating conditions of the synthesis process leading to the production of TiO₂-carbon nanopowder with reduced adverse health effect.

1. Introduction

Titanium dioxide (TiO₂) can be considered as one of the most used materials in the modern era, since it is suitable for a large number of applications in several different fields. As bulk material, TiO₂ is produced in the order of millions of tons per year, and it is mainly used as a white pigment in plastics and paintings. As a nanomaterial, its unusual properties entail a wide range of applications (Kamat, 2012), which span from photocatalyst for water splitting and air purification (Ni et al., 2005) to food color additive and component in personal care products (Weir et al., 2012). A huge number of flame synthesis configurations have been used over the years to produce titanium dioxide nanostructures, showing that the experimental set-up and the operating conditions can be varied to gain a control on crystalline phase, size and morphology of synthesized nanoparticles.

Concerning personal care products area, a widespread application is physical filter for sun-screen. Indeed, titania optical properties make it able to absorb both UVB (290–320 nm) and UVA (320–400 nm) radiations, which are mostly responsible of skin damages deriving from sun exposure (Smijs and Pavel, 2011). Also, advantages offered by sunscreens based on TiO₂ nanoparticles comprise the reduction of skin irritation and

sensitization with respect to sunscreens made of organic compounds and the elimination of the natural opacity of microsized sunscreen without reducing UV blocking efficacy.

A fundamental requirement for using titania in sunscreens and other personal care products is photostability. Under UV illumination in aqueous media, photoactive TiO₂ can induce the formation of Reactive Oxygen Species (ROS), which are responsible of skin DNA and RNA damages (Hirakawa et al., 2004).

Several methods have been studied to improve the stability of TiO₂ nanoparticles under UV illumination, such as doping and coating of nanoparticles surface with inorganic and/or organic substances (Lee et al., 2007). Recently, Livraghi et al. (2010) showed that the modification of TiO₂ nanoparticles with carbon induced the depression of ROS formation and so the reduction of nanopowder skin toxicity.

The aim of this study was to produce by flame synthesis and to characterize pure titania nanopowder and carbon-titania nanopowder for cosmetic applications, in order to investigate the possible reduced health effects in terms of ROS production given by the addition of carbon to titania nanopowder.

2. Experimental

The aerosol flame synthesis set-up consists of the combination of a Berglund Liu type Vibrating Orifice Aerosol Generator (VOAG, TSI 3450) and a honeycomb burner. The burner was composed by an 18 mm ID stainless steel tube, with 26 mm long Mullite Zirconia Honeycomb (400 CPSI) placed on its top, used to stabilize the flame. The burner had an outside ring (ID 24 mm, OD 34 mm) used to flow sheath Argon (65 NI/hr) to isolate the flame from the surrounding air. Burner walls were equipped with electrical resistances controlled by a proportional-integrated controller. A 0.3 M solution of titanium tetraisopropoxide (TTIP, Aldrich, 97%) into ethanol was used as precursor. VOAG generated a uniform droplets jet, which was then dispersed into an air stream and injected directly into the burner. The burner walls were heated to 450 K to ensure complete evaporation of both ethanol and TTIP before reaching the flame front. Ethylene was used as fuel, with air as oxidant to generate a burned stabilized, flat, atmospheric premixed flame. Two different experimental flame conditions were investigated, as reported in Table 1.

Table 1: Experimental flame conditions

	Ethylene, NI/hr	Air, NI/hr	Ethanol, NI/hr	Cold Gas Velocity, cm/s	Flame Equivalent Ratio ϕ
Flame_1.52	10	220	17.5	27	1.52
Flame_1.73	10	190	17.5	24	1.73

Particles were collected by thermophoresis on a chilled stainless steel plate. XRD spectra were recorded on a Bruker D2 Phaser X-Ray Powder Diffractometer operated with a Cu(K α) radiation, while Raman analysis was performed with a Horiba XploRA Raman Microscope System. Powders morphology was observed by means of Scanning Electron Microscopy (SEM, Philips XL30, LaB6 filament).

AFM measurements were performed with a Scanning Probe Microscope NTEGRA Prima from NT-MDT at room temperature and 30% relative humidity, operated in semi-contact mode in air using NANOSENSORS™ SSS-NCHR super-sharp silicon probes with nominal tip radius of 2 nm, over selected areas of 8 μ m \times 6 μ m (1024 \times 1024 pixel resolution).

For optical analysis, nanoparticles were collected on quartz substrates, and UV-visible spectra were measured in the wavelength range 200–700 nm by means of a Spectrophotometer Agilent 8453, coupled with Agilent UV-Vis ChemStation.

ROS detection was performed on human keratinocytes cells (HaCaT), grown in Dulbecco's modified Eagle's medium (DMEM) medium with 1% L-glutamine (Lonza), 1% penicillin/streptomycin (Lonza), and 10% foetal calf serum (Gibco). For control wells (untreated cells), a corresponding amount of compound buffer was added. To induce ROS, the cell plate was incubated in a 5% CO₂, 310 K atmosphere for one hour. Fluorescence intensity, proportional to the amount of ROS present, was measured at $\lambda_{ex}=520$ nm/ $\lambda_{em}=605$ nm with a Tecan Infinite 200 PRO Microplate Reader.

3. Results and Discussion

Characterization of flame temperature was carried out using an R-type thermocouple (Pt/13%Rh vs. Pt), substituting TTIP solutions with pure ethanol to prevent nanoparticles deposition on thermocouple junction. Flame temperature was measured every 5 millimeters above the burner from 7.5 cm (Flame_1.52) and from 5 cm (Flame_1.73) up to 9.8 cm; just below the sampling plate. Below 7.5 cm for Flame_1.52 and 5 cm for

Flame_1.73, temperature reached a value higher than 2000 K, which is above the maximum operating level of the thermocouple. Temperature measurements are corrected for radiation losses (McEnally et al., 1997). The profiles are reported in Fig. 1.

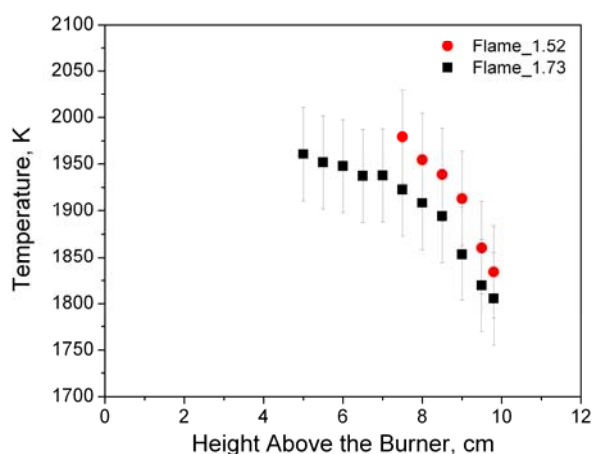


Figure 1: Temperature profiles measured for the studied flames. Error bars report the uncertainty in the temperature of ± 50 K.

XRD is a well-established technique to determine the phase of TiO_2 particles. The XRD spectra measured for powders produced in the two different flame conditions are reported in Fig. 2a. It can be observed that synthesized powders have both rutile and anatase phases, rutile being the predominant phase. The weight fraction of the rutile phase has been calculated from the ratio between the relative intensities of the most intense peaks for anatase and rutile (Spurr and Myers, 1957) to be 85% for nanoparticles coming from Flame_1.52 and 91% for nanoparticles coming from Flame_1.73. Those findings are in agreement with the results of Memarzadeh et al. (2011), which showed that fuel-rich conditions favor the formation of rutile phase, while anatase-phase TiO_2 particles typically grow in highly oxygen-rich environments (Kho et al., 2011). The average crystal dimensions have been estimated from XRD analysis by the Scherrer equation (Cullity, 1968) to be 40 nm (rutile phase) and 30 nm (anatase phase) for particles produced in Flame_1.52 conditions and 37 nm (rutile phase) and 27 nm (anatase phase) for particles produced in Flame_1.73 conditions.

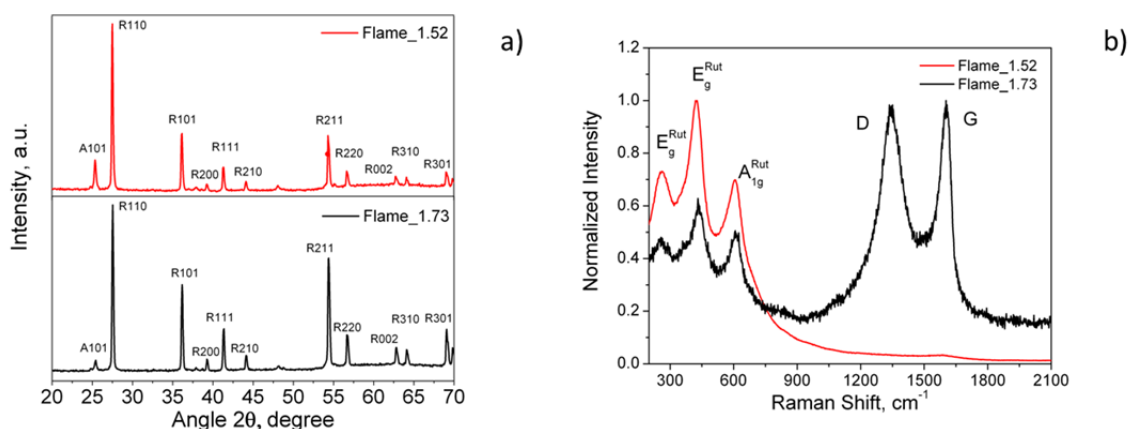


Figure 2: XRD patterns (a) and Raman spectra (b) of titania nanopowder produced from Flame_1.52 (red curve) and Flame_1.73 (black curve).

Raman spectra in the visible region of synthesized nanopowders are reported in Fig. 2b. In both samples, the peaks corresponding to the two E_g modes (235 cm^{-1} and 447 cm^{-1}) and to the A_{1g} mode (612 cm^{-1}) of rutile are present (Ohsaka et al., 1978). In addition, the sample coming from Flame B shows the presence of two additional peaks: the G-peak (1580 cm^{-1}), which has been observed in graphitic type structures, and the D-

peak (1360 cm^{-1}), which occurs due to defects in graphitic structures. Those peaks clearly show that carbon growth occurs together with titania nanoparticles synthesis when particles are produced in Flame_1.73 conditions.

Dimensional characterization was performed by means of AFM on isolated particles collected by thermophoresis with a single insertion. AFM images were acquired over an area of $8\text{ }\mu\text{m} \times 8\text{ }\mu\text{m}$ and then analyzed to obtain volume, base area and maximum height of the particles. Particle volume was evaluated from the base diameter and height considering a conical shape, and the distribution of the diameter D_p of spheres with equal volume was finally determined (De Falco et al., 2015). The particle size distributions (PSDs) were then fitted by a lognormal distribution function (Hinds, 1999), shown in Equation 1:

$$\frac{1}{N} \frac{dN}{d\ln D_p} = \frac{1}{\sqrt{2\pi} \ln(\sigma)} \exp\left(-\frac{\ln(D_p / \langle D_p \rangle)^2}{2 \ln(\sigma)^2}\right) \quad (1)$$

Where D_p is the particle diameter, $\langle D_p \rangle$ is the mean particle diameter, N is the number density of the particles and σ is the geometric standard deviation.

Fig. 3 reports the particle equivalent diameter distributions obtained from AFM for the two flame conditions, together with their best fit from Equation 1. Mean particle diameters were calculated to be 30.5 nm for Flame_1.52 and 29 nm for Flame_1.73, in good agreement with average crystal dimensions obtained from XRD data.

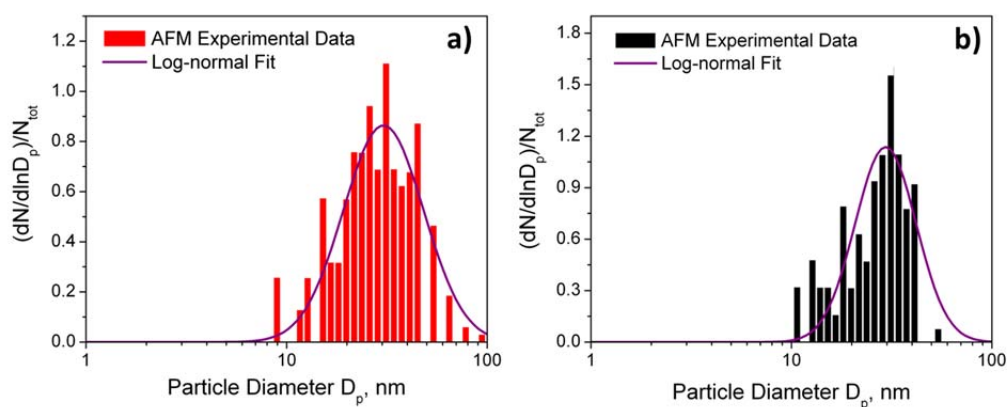


Figure 3: PSDs from AFM of pure-titania powder from Flame_1.52 (a, red bars) and carbon-titania powder from Flame_1.73 (b, black bars), and best log-normal fit curves from Eq. 1 (purple lines).

Properties of synthesized particles were also investigated using phase mode imaging. AFM phase mode images of pure-titania and carbon-titania nanoparticles from Flame_1.52 and from Flame_1.73 are shown in Fig. 4. Changes in the phase of cantilever oscillation, caused by changes in the investigated material properties (viscoelasticity, hardness and stickiness), result in a relative phase lag map, in which dark areas correspond to a negative phase lag, while bright areas correspond to a positive phase lag. The images show that nanoparticles from Flame_1.52 are characterized by a negative phase lag, surrounded by a bright edge area, while nanoparticles from Flame_1.73 are characterized by a positive phase lag, surrounded by a dark edge area. Unfortunately, it is not possible to obtain quantitative information from phase images, but they are a clear evidence of differences in surface properties between pure-titania and carbon-titania nanoparticles.

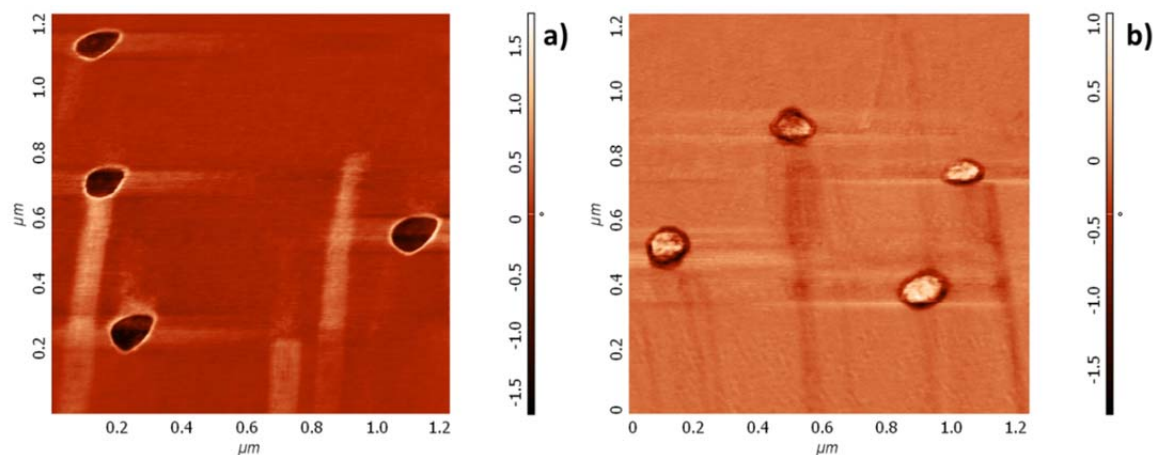


Figure 4: AFM phase mode images of pure-titania nanoparticles from Flame_1.52 (a) and carbon-titania nanoparticles from Flame_1.73 (b).

UV-Vis absorption spectra of the two nanopowders are reported in Fig. 5. Both nanopowders show a high absorption efficiency in the UVA and in the UVB regions, while absorption in the visible region at $\lambda > 400$ nm is significantly increased for carbon-titania nanopowder.

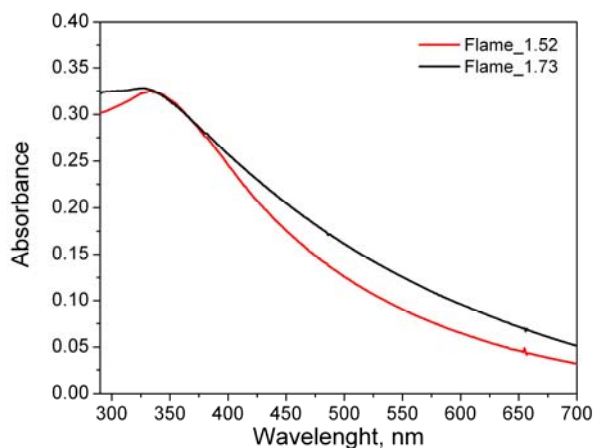


Figure 5: UV-Vis absorption spectra of pure-titania powder Flame_1.52 and from carbon-titania powder from Flame_1.73.

The analysis of Reactive Oxygen Species production was performed on HaCaT cells exposed to a concentration of 5 $\mu\text{g}/\text{ml}$ of three different TiO_2 powder: pure TiO_2 powder produced in Flame_1.52, carbon- TiO_2 powder produced in Flame_1.73, and commercial titania nanopowder (Sigma Aldrich, <100 nm particle size). Figure 6 reports the fluorescence intensity signals measured after one-hour treatment, which is proportional to the amount of generated ROS. It is possible to observe that flame-synthesized titania produces a lower amount of ROS with respect to commercial TiO_2 . Also, the presence of carbon induces a positive effect, which results in further reduction of the ROS produced by the cells.

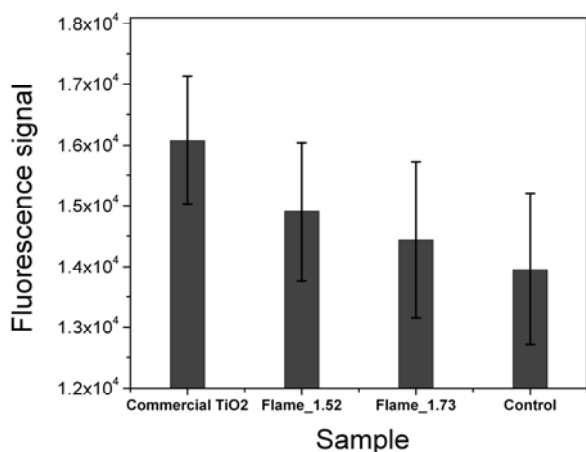


Figure 6: Intracellular ROS generation after treatment of HaCaT cells with commercial TiO₂ nanopowder, Flame_1.52 pure-TiO₂ nanopowder and Flame_1.73 carbon-TiO₂ nanopowder.

4. Conclusions

In this work, pure and TiO₂-carbon nanoparticles have been produced by flame synthesis in a premixed flame reactor, operated with two different equivalent ratio and cold gas velocity, in order to synthesize pure TiO₂ and carbon-TiO₂ nanoparticles with similar dimension and compositions. Crystallinity and phase analysis was performed by XRD, showing that both nanopowders are composed by a mixture of anatase and rutile, as expected in fuel-rich conditions, with an 85%/90% content of rutile which is the preferable phase for cosmetic application, due to its lower photoactivity. The presence of carbon in the synthesized carbon-TiO₂ powder was confirmed by Raman spectroscopy. Particle dimensions and morphology were derived from AFM, while acquired UV-Vis spectra showed that both nanopowders give a scattering contribution which enhances the protection in the UVA region. ROS analysis showed that the presence of carbon induces a reduction of ROS production in human keratinocytes cells by titania nanopowders.

References

- Cullity, B.D., 1978, Elements of X-ray diffraction (2nd ed.), Addison Wesley, Reading, United Kingdom.
- De Falco, G., Commodo, M., Minutolo, P., D'Anna, A., 2015, Aerosol Sci. Technol. 49 (5), 281-289.
- Hinds, W. C., 1999, Aerosol technology: properties, behavior and measurements of airborne particles, Wiley-Interscience, New York, USA.
- Hirakawa, K., Mori, M., Yoshida, M., Oikawa, S., Kawanishi, S., 2004, Free Radical Res. 38, 439-447.
- Kamat, P.V., 2012, J. Phys. Chem. C 116, 11849-11851.
- Kho, Y.K., Teoh, W.Y., Mädler, L., Amal, R., 2011, Chem. Eng. Sci. 66 (11), 2409-2416.
- Lee, W.A., Pernodet, N., Li, B., Lin, C. H., Hatchwell, E., Rafailovich, M.H., 2007, Chem. Commun. 45, 4815-4817.
- Livraghi, S., Corazzari, I., Paganini, M.C., Ceccone, G., Giamello, E., Fubini, B., Fenoglio, I., 2010, Chem. Commun. 46 (44), 8478-8480.
- McEnally, C.S., Koylu, U.O., Pfefferle, L.D., Rosner, D.E., 1997, Combust. Flame 109 (4), 701-720.
- Memarzadeh, S., Tomalchoff, E.D., Phares, D.J., Wang, H., 2011, Proc. Combust. Inst. 33, 1917-1924.
- Ni, M., Leung, M.K.H., Leung, D.Y.C., Sumathy, K., 2007, Renew. Sustain. Energy Rev. 11, 401-425.
- Ohsaka, T., Izumi, F., Fujiki, Y., 1978, J. Raman Spectrosc. 7, 321-324.
- Smijjs, T.G., Pavel, S., 2011, Nanotechnol. Sci. Appl. 4, 95-112.
- Spurr, R.A., Myers, H., 1957, Anal. Chem. 29, 760-762.
- Weir, A., Westerhoff, P., Fabricius, L., Hristovski, K., von Goetz, N., 2012, Environ. Sci. Technol. 46, 2242-2250.